

# Characterization of the Hydrochlorothiazide: $\beta$ -Cyclodextrin Inclusion Complex. Experimental and Theoretical Methods

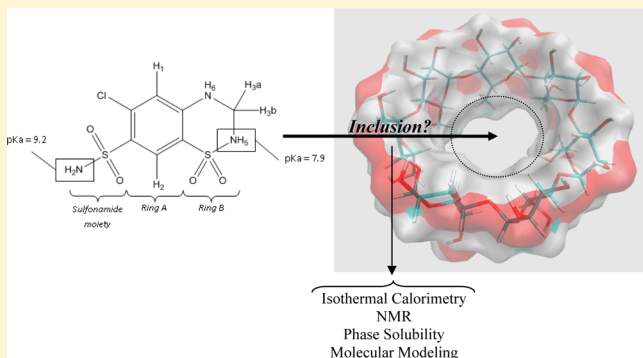
Renée Onnainty,<sup>†</sup> Esteban M. Schenfeld,<sup>†</sup> Mario A. Quevedo,<sup>†</sup> Mariana A. Fernández,<sup>‡</sup> Marcela R. Longhi,<sup>†</sup> and Gladys E. Granero\*,<sup>†</sup>

<sup>†</sup>Departamento de Farmacia, UNITEFA, CONICET, Facultad de Ciencias Químicas, Universidad Nacional de Córdoba, Córdoba, X5000HUA, Argentina

<sup>‡</sup>Departamento de Química Orgánica, INFIQC, CONICET, Facultad de Ciencias Químicas, Universidad Nacional de Córdoba, Córdoba, X5000HUA, Argentina

## Supporting Information

**ABSTRACT:** Hydrochlorothiazide (HCT) is one of the most commonly prescribed antihypertensive drugs. In an attempt to gain an insight into the physicochemical and molecular aspects controlling the complex architecture of native  $\beta$ -cyclodextrin ( $\beta$ -CD) with HCT, we performed multiple-temperature–pH isothermal titration calorimetric measurements of the HCT:  $\beta$ -CD system, together with proton nuclear magnetic resonance spectroscopy ( $^1\text{H}$  NMR), phase solubility analysis, and molecular modeling methods. The  $A_{\text{L}}$ -type diagrams, obtained at different pH values and temperatures, suggested the formation of soluble 1:1 inclusion complexes of  $\beta$ -CD with HCT. The corresponding stability constants ( $K_{1:1}$ ) were determined by phase solubility studies and compared with those obtained by ITC, with good agreement between these two techniques being found. The three-dimensional array of the complex was studied by  $^1\text{H}$  NMR and molecular modeling methods. Both techniques confirmed the formation of the inclusion complex, with good agreement between the experimental and theoretical techniques regarding the HCT binding mode to  $\beta$ -CD. Also, the forces involved in the association process were determined, both from the thermodynamic parameters obtained by ITC (association enthalpy, binding constant, Gibbs free energy, and entropy) and from energetic decomposition analyses derived from computational methods. We concluded that the formation of the HCT:  $\beta$ -CD complex was enthalpy driven, with the inclusion mode of HCT being highly dependent on its ionization state. In all cases, sustained hydrogen bond interactions with hydroxyl groups of  $\beta$ -CD were identified, with the solvation energy limiting the affinity. Regarding the pH and temperature dependence, lower affinity constants were found at higher HCT ionization states and temperatures.



## INTRODUCTION

Cyclodextrins (CD) are well-known molecular hosts in supramolecular chemistry, being cyclic oligosaccharides composed of six, seven, or eight glucose units that are referred to as  $\alpha$ -,  $\beta$ -, and  $\gamma$ -cyclodextrin, respectively. CDs are able to form inclusion complexes with a great variety of organic substances, either in solution or in the solid state, a feature that may lead to enhanced pharmaceutical and biopharmaceutical properties of drugs, such as increased solubility and stability.<sup>1–3</sup> For this reason, they have been widely used in many fields such as the pharmaceutical industry,<sup>4–6</sup> food technology,<sup>7,8</sup> biotechnology,<sup>9</sup> cosmetics,<sup>10</sup> and analytical chemistry.<sup>11</sup> The phenomena underlying the formation of the inclusion complex involves several noncovalent intermolecular forces, such as hydrophobic ones, hydrogen bonds, and dipole–dipole, ion–dipole, and van der Waals interactions, while conformational energy contributions are also frequent.<sup>12–14</sup> In addition, the solvent behavior (i.e., water molecules) determines the mode and spontaneity of the complex formation, with solvation energies frequently limiting host molecule affinities.<sup>15</sup>

Also, the interaction between CDs and several ligands of pharmaceutical relevance has also been studied in detail at the unimolecular level,<sup>16,17</sup> stressing the importance of the intermolecular interaction in the observed binding constant. Therefore, investigation of the physicochemical properties and intermolecular forces that underlie the complexation event, as well as the structural characterization of these inclusion complexes at atomic level, is of great importance to be able to rationalize the use of CD aimed at pharmacotherapeutic goals. Furthermore, the possibility of modulating the affinity of drugs included in CD is a key feature in drug delivery strategies,<sup>18</sup> since the CD must be able to bind the drug strongly enough to efficiently deliver it to the desired target (frequently absorption sites), while at the same time it must be weak enough to allow the drug to be released upon its arrival at that site. Thus, a detailed

Received: November 14, 2012

Revised: December 12, 2012

Published: December 13, 2012

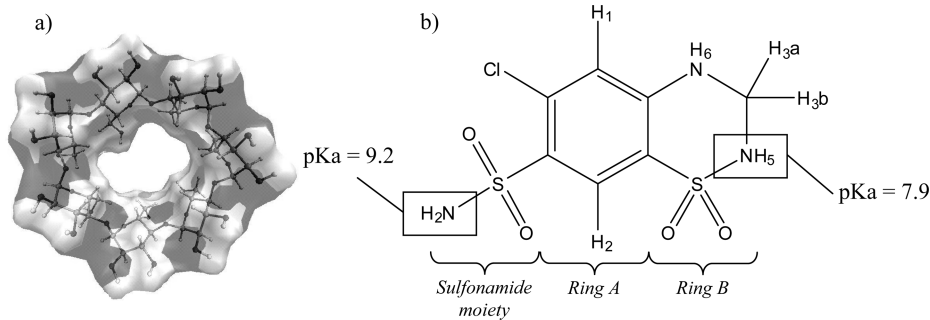


**Figure 1.** (a) Three-dimensional structure of  $\beta$ -CD and (b) chemical structure of hydrochlorothiazide showing the  $pK_a$  values for the corresponding acidic groups.

understanding of the features that contribute to the complex stability during the drug's administration and presence in the organism are essential for the design of drug:CD complexes with potential pharmacotherapeutic use. From a physicochemical point of view, some of the most relevant aspects that may be assessed include the effect of pH, drug:CD mole ratio, and temperature.

Among the CDs,  $\beta$ -CD is the most widely used, with this molecule often being described as a shallow truncated cone with hydrophilic exterior and a hydrophobic interior cavity (Figure 1a and Figure S1 in the Supporting Information).<sup>1,3</sup> Several reports have highlighted the ability of  $\beta$ -CD to reach different goals of pharmaceutical relevance,<sup>19–21</sup> of which the possibility of protecting the included drug against metabolism and enhancing its solubility constitute the main applications.<sup>22–24</sup>

Hydrochlorothiazide (HCT, 6-chloro-3,4-dihydro-2*H*-1,2,4-benzothiadiazine-7-sulfonamide-1,1-dioxide, Figure 1b) is a diuretic agent that has become the most commonly prescribed antihypertensive drug in the United States.<sup>25</sup> Taking into account that HCT exhibits a low solubility in water (being classified in the Biopharmaceutical Classification System as a class II compound),<sup>26</sup> several approaches have been envisioned to increase its solubility and bioavailability.<sup>27,28</sup> So, the formation of inclusion complexes between HCT and  $\beta$ -CD appears a very promising way of enhancing these pharmaceutical properties, and thus the elucidation of the physicochemical and molecular properties that drive this complexation may provide a further rational basis for controlling the complex behavior. Taking into account that HCT is a diacid, the effect of the degree of drug ionization on its affinity for  $\beta$ -CD also merits detailed analysis.

The thermodynamic characterization for the formation of HCT:CD inclusion complexes by means of NMR spectroscopy, isothermal titration calorimetry (ITC), and quasi-elastic light scatter has been previously explored by Denadai et al.<sup>29</sup> However, these investigations were restricted to an aqueous environment, and thus no further conclusions regarding the pH dependence on HCT affinity could be drawn since the neutral form of HCT may be assumed to have been present. Moreover, no molecular details regarding the driving forces responsible for the formation of the complexes, or of their structural features at the local minima of the free-energy surface, were reported. Consequently, the HCT: $\beta$ -CD interaction mechanism is still poorly known, and thus merits further investigation by the application of state of the art experimental and theoretical methodologies.

In the context of the above-mentioned topics, we carried out a large number of isothermal titration calorimetric (ITC) measurements at different temperatures and pH values with the choice of ITC being based on the fact that it is recognized as a

reference technique for the thermodynamic characterization of complex formation.<sup>30</sup> Also, results derived from phase solubility analyses are presented, as this technique constitutes one of the most commonly applied ones to study CD complexation and to determine the stoichiometry of the inclusion complex.<sup>5</sup> To assess the three-dimensional structure of the complex, <sup>1</sup>H NMR, molecular docking, molecular dynamics, and free energy decomposition analyses were also applied. These computational techniques include a wide range of tools that are able to model at atomic resolution the interaction between host and guest molecules.<sup>31–34</sup> Furthermore, these techniques have been widely applied to study at atomic resolution the energetics, physicochemical properties, and structure of inclusion complexes involving  $\beta$ -CD.<sup>35–37</sup>

## EXPERIMENTAL AND THEORETICAL METHODS

**Reagents and Materials.** HCT was purchased from Parafarm (Buenos Aires, Argentina) and used without further purification.  $\beta$ -CD was a gift from Ferromet S.A. (agent of Roquette in Argentina). The D<sub>2</sub>O 99.9% D used in the spectroscopic studies was purchased from Sigma (Buenos Aires, Argentina). All experiments were performed with analytical grade chemicals. The water used in these studies was generated with a Milli-Q Water Purification System (Millipore, Bedford, MA). Phosphate buffer solution was used to control the pH value of the media.

**Isothermal Titration Calorimetry (ITC).** ITC experiments were performed at 293, 298, 310, and 318 K, using a VP-ITC Microcalorimeter (MicroCal, Inc., Northampton, MA). For each experiment, 28 aliquots of a  $\beta$ -CD-buffered solution (10  $\mu$ L each) were titrated into the reaction cell (1.4542 mL) containing the HCT-buffered solutions (pH = 3.0, 5.5, 6.8, 7.4, 8.0, and 10.0). The initial guest concentration for all experiments was 2.0 mM (titration cell), while the initial host concentration in the infusion syringe was 12 mM. During the experiment and as a consequence of sample dilution in the titration cell, the guest concentration varied between 2.0 and 1.67 mM, while host concentrations ranged from 0 to 2.0 mM, and all solutions were degassed prior to starting the measurements. The aliquots were added at 3.3 min intervals to allow the solution in the cell to equilibrate after each addition. Before each binding assay, the heat of dilution of  $\beta$ -CD was measured by titrating 28 aliquots (10  $\mu$ L each) into the corresponding buffer (pH = 3.0, 5.5, 6.8, 7.4, 8.0, and 10.0) and the assay temperature was recorded. Data obtained from the experiments were processed and afterward converted into binding isotherms. Prior to model fitting, the heat of dilution was subtracted from the isotherms corresponding to the heat of binding. The first injection (5.0  $\mu$ L) was discarded to account for any material diffusion effects between the syringe and calorimetric cell. Each experiment was

carried out in triplicate to ensure reproducibility, with data from replicate experiments observed to exhibit differences of less than 10%. Binding enthalpies ( $\Delta H^\circ$ , kJ·mol<sup>-1</sup>), stoichiometry ( $n$ ), and binding constants ( $K$ , M<sup>-1</sup>) were obtained by nonlinear fitting using MicroCal Origin software provided with the instrument.

**NMR Studies.** All experiments were performed on a Bruker Avance II 400 (400.16 MHz), high resolution spectrometer, equipped with a broad band inverse probe (BBI) and a variable temperature unit (VTU). Spectra were measured at 298 and 318 K in phosphate buffer (0.2 M)/D<sub>2</sub>O (8/2), adjusting the pH value at 3.0, 5.5, 7.4, 8.0, 8.7, 9.5, 10, and 12 with sodium hydroxide or D<sub>2</sub>O. The chemical shift of the residual solvent at 4.8 ppm was used as an internal reference. Due to its low solubility, solutions containing HCT or HCT plus  $\beta$ -CD were prepared as follows: an excess of HCT was added to 5 mL of an aqueous solution of  $\beta$ -CD (12 mM) in phosphate buffer (0.2 M)/D<sub>2</sub>O (8/2) or D<sub>2</sub>O, which was afterward subjected to mechanical shaking for 24 h at 298 K. The resulting suspensions were filtered before performing <sup>1</sup>H NMR analyses.

The  $\Delta\delta$  in the <sup>1</sup>H chemical shift for  $\beta$ -CD and HCT originated by the complexation phenomena was calculated applying the following eq 1:

$$\Delta\delta = \delta_{\text{complex}} - \delta_{\text{free}} \quad (1)$$

**Phase Solubility Analyses.** Phase solubility studies were carried out according to a method described by Higuchi and Connors.<sup>38</sup> An excess amount of HCT was mixed in a series of buffer solutions (pH 3, 5.5, 6.8, 7.4, 8, 10) containing increasing amounts of  $\beta$ -CD (0–12 mM) and subjected to vortex mixing. After dissolution the equilibrium was reached. Then, samples were filtered through 0.45  $\mu$ m membrane filters, and after the resulting pH was measured, appropriate dilutions were performed to quantify HCT by UV spectrophotometry at 270 nm. The UV absorption of  $\beta$ -CD was negligible at the assay wavelength. All measurements were done at 298, 310, and 318 K, with the apparent stability constants ( $K$ , M<sup>-1</sup>) being calculated from the corresponding phase solubility diagrams using eq 2

$$K = \frac{\text{slope}}{S_0(1 - \text{slope})} \quad (2)$$

where  $S_0$  represents the intrinsic solubility of the drug.

Each experiment was performed in triplicate, with the mean ( $\pm$ SD) being reported.

**Statistical Analyses.** The statistical significance of differences between the  $K_{1:1}$  constants obtained by ITC and those of the phase solubility studies was estimated using the Student's *t*-test. Differences were considered to be statistically significant at  $p < 0.05$ .

**Molecular Modeling.** The initial structure of HCT was built using the Gabedit software,<sup>39</sup> after which conformational and energetic analyses were performed with the Gaussian03 software.<sup>40</sup> The corresponding minimum-energy conformation was obtained by applying a systematic conformational search based on semiempirical (AM1) methods, with the final minimum-energy conformation being optimized using an ab initio (HF-6-31G\*) method. The restrained electrostatic potential (RESP) fitted charges model was applied to the final optimized geometry, which was also used to model the electrostatic interactions between HCT and  $\beta$ -CD.

Complexes between HCT and  $\beta$ -CD under the different simulated conditions were predicted by molecular docking, using software packages developed by OpenEye Scientific Software.<sup>41</sup>

Initial structures of the ligands were obtained as previously mentioned, while the structure of  $\beta$ -CD was retrieved from the Cambridge Structural Database (code BCDEXD10). The molecular docking procedures consisted of three phases: (a) ligand conformer library generation and parametrization, which was performed using OMEGA software,<sup>42,43</sup> by assuming an energy threshold of 10 kcal/mol; (b) the docking assay, which was performed applying a fast rigid exhaustive docking approach as implemented in the FRED3 and the OEDocking suite;<sup>44–46</sup> the ChemGauss3 force field was used to score HCT binding to  $\beta$ -CD, with the best 10 docked poses being reported; (c) visualization and analysis were carried out using the VIDA v.4.2.1 software,<sup>41,47</sup> selecting the corresponding docking poses that were then subjected to further molecular dynamics analyses.

The Amber12 software package was used for the molecular dynamics (MD) studies.<sup>48</sup> Atomic charges and molecular parameters corresponding to HCT were assigned from the GAFF force field,<sup>49</sup> while those corresponding to  $\beta$ -CD corresponded to the GLYCAM\_06 force field.<sup>50</sup> To perform these simulations, the complexes obtained by molecular docking were used as initial structures, solvated with a pre-equilibrated TIP3P cubic box of explicit water molecules, and subjected to minimization. The minimized systems were then heated to the target temperatures (298, 310, and 318 K) for 20 ps, using a time step of 2 fs under constant pressure and temperature conditions. The SHAKE algorithm was applied to constrain bonds involving hydrogen atoms. After the system was heated, an equilibration phase (1 ns) was performed followed by the corresponding production phase (10 ns).

Analyses of the MD trajectories were carried out using the Cpptraj module of Amber12, with energetic decomposition analyses being performed by applying the molecular mechanics Poisson–Boltzmann surface area (MM-PBSA) approach.<sup>51</sup> The resulting trajectories were visualized using VMD v.1.9 software.<sup>52</sup> Molecular dynamics trajectories were obtained using CUDA designed code (*pmemd.cuda*), with computational facilities provided by the GPGPU Computing group at the Facultad de Matemática, Astronomía y Física (FAMAF), Universidad Nacional de Córdoba, Argentina.

## RESULTS AND DISCUSSION

**ITC Experiments.** In order to estimate the enthalpy, the entropy changes and corresponding affinity constants associated to the formation of the HCT: $\beta$ -CD inclusion complex, calorimetric measurements were conducted under the experimental conditions detailed in section 2.2.

Titration microcalorimetry permits the simultaneous determination of the equilibrium constant, enthalpy, and complex stoichiometry from a single titration curve using the least-squares nonlinear adjustment based on the Wiseman isotherm (eq 4).<sup>53,54</sup>

For the most simple case of a 1:1 ligand–receptor (X–M) binding



the Wiseman isotherm (eq 4) relates the stepwise change in the heat of the system (normalized with respect to the moles of the ligand added per injection ( $dQ/d[X]_t$ )) to the absolute ratio of the ligand to the receptor concentration ( $X_R = [X]_t/[M]_t$ ), at any point over the course of the titration. The parameters  $\Delta H^\circ$ ,  $V_0$ , and  $r$  are respectively the molar enthalpy of binding, the effective volume of the solution in the titration cell, and the composition variable  $1/[CD]TK_{\text{eq}}$ .

$$\frac{dQ}{d[X]_t} = \Delta H^\circ V_0 \left[ \frac{1}{2} + \frac{1 - X_R - r}{2\sqrt{(1 + X_R - r)^2 - 4X_R}} \right] \quad (4)$$

where

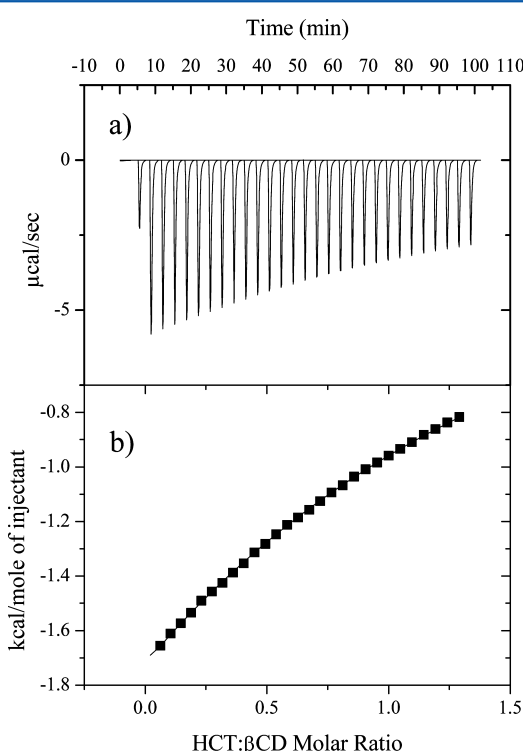
$$\frac{1}{r} = c = K_a [M]_t = \frac{[M]_t}{K_d} \quad (5)$$

Applying eqs 6 and 7, it is possible to calculate the free energy and entropy parameters.

$$\Delta G^\circ = -RT \ln K \quad (6)$$

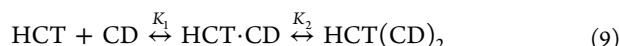
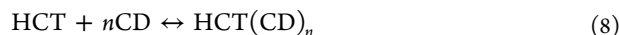
$$\Delta G^\circ = \Delta H^\circ - T\Delta S^\circ \quad (7)$$

Figure 2 shows a representative plot of the heat exchange versus HCT: $\beta$ -CD molar ratio for a solution of HCT that was



**Figure 2.** (a) Variation of the heat flow as a function of time; (b) rate of change in the corresponding heat caused by the host–guest interactions versus concentration ratio of host to guest.

titrated with a solution of  $\beta$ -CD. In order to determine the type of interaction that best fitted the experimental data, the one-site and sequential binding models were evaluated, with  $n$ ,  $k$ , and  $H$  representing adjustable parameters. These two models correspond to the reactions indicated in eqs 8 and 9, and are implemented in the software as a “single-site model” and “sequential binding model”, respectively.



The best fit was obtained assuming the single-site model, with the results summarized in Table 1. In all cases, an exothermic reaction was observed while the stoichiometry of the complex was 1:1.

From the calculated thermodynamic parameters, it can be seen that the decrease of Gibbs energy ( $\Delta G^\circ$ ) associated to the

inclusion complex formation was mainly enthalpy driven. This exothermic phenomenon was related to the intermolecular interactions that were established between HCT and  $\beta$ -CD upon complexation, and resulted in both favorable and unfavorable thermodynamic events. It is known that van der Waals interactions constitute a key component that drives the  $\beta$ -CD inclusion complex formation, so it was expected that HCT would position the most hydrophobic part of the molecule inside the cavity of  $\beta$ -CD, while the more polar moieties would be exposed to the solvent. It is also known that dehydration plays an important role in inclusion to  $\beta$ -CD,<sup>15</sup> with the energetic cost of this event also being accounted for in the observed enthalpy change. Considering that the binding of HCT exhibited negative  $\Delta G^\circ$  values, it was expected that stabilization conferred by the van der Waals and electrostatic interactions would compensate for the energetic cost of dehydration. Also, the enthalpic change associated to the complex formation was highly dependent on the ionization state of HCT and temperature, with lower values being obtained at higher ionization states and temperatures, suggesting that the intermolecular interactions between HCT, and thus the complex structure, were highly modified by these variables. This observation is consistent with the general rule seen in the literature, where a charged ligand exhibits lower affinity constants for  $\beta$ -CD than its corresponding un-ionized counterpart. The identification at atomic level of this phenomenon will be further discussed as part of the molecular modeling studies.

Regarding the entropy change ( $\Delta S$ ), low negative values were found, which were originated from the conformational rearrangement and desolvation associated with the complex formation. It may be that, upon complex formation, the water molecules are excluded from the  $\beta$ -CD cavity and binding interface, which in turn originates significant solvent reorganization. The negative entropy change observed may have originated from the entropic gain derived from the rearrangement of the water molecules originally surrounding the host and guest molecules, with the entropic loss of the ligand being related to the decrease in the motion freedom upon complexation. As these opposed effects were nearly equal, the variation in entropy was low, and in this particular case slightly negative.

The effect of temperature on HCT affinity for  $\beta$ -CD was also analyzed, with the affinity being lowered as the temperature was raised. Although it has been proposed in the literature that inclusion complexes dissociate when temperature is increased,<sup>55</sup> the identification of the molecular aspects behind this behavior has not yet been established.

**<sup>1</sup>H NMR Studies.** NMR spectroscopy permits the study of the environment of individual atom nuclei through the quantitation of the variation of the chemical shifts of various proton signals, and thus it is possible to establish relevant inferences regarding the ligand inclusion mode. In this way, the inclusion of HCT into the  $\beta$ -CD cavity was first evaluated by measuring the changes in the chemical shifts ( $\Delta\delta$ ) of the protons in the complex, relative to the free HCT and  $\beta$ -CD, at different pH values (3–12) and temperatures (298–318 K). Tables 2–4 show the assignments of the HCT and  $\beta$ -CD peaks along with the  $\Delta\delta$  due to complexation (see proton numbering in Figure S1 in the Supporting Information).

It is well-known that  $\beta$ -CD molecules adopt the conformation of a torus, in which the  $H_3$  and  $H_5$  protons are located inside the cavity, whereas  $H_2$  and  $H_4$  are on the outside. The  $H_6$  protons of the primary alcohol group are on the narrower side, while  $H_1$  lies on in the glycosidic bond plane of the  $\beta$ -CD

**Table 1.** Values of the Stability Constant ( $K$ ) and Thermodynamic Parameters for the HCT: $\beta$ -CD Complex Determined by Isothermal Titration Calorimetry (ITC) and Phase Solubility Analysis (DSP) under Different Experimental Conditions (pH and Temperature)

pH	T (K)	ITC				DSP	
		$K$ ( $M^{-1}$ )	$\Delta H^\circ$ (kJ·mol $^{-1}$ )	$\Delta G^\circ$ (kJ·mol $^{-1}$ )	$\Delta S$ (J·mol $^{-1}$ ·K $^{-1}$ )	$K$ ( $M^{-1}$ )	$p > 0.05$
3	293	158 ± 1	-29.6 ± 0.2	-12.4	-59.0	nd	-
	298	110 ± 1	-39.8 ± 0.3	-11.6	-71.1	123 ± 5	0.10
	310	79 ± 1	-29.3 ± 0.2	-11.1	-58.2	114 ± 6	0.07
	318	70 ± 1	-24.5 ± 0.4	-11.2	-41.8	42 ± 8	0.05
5.5	293	168 ± 2	-25.6 ± 0.2	-17.1	-26.8	nd	-
	298	115 ± 1	-32.2 ± 0.2	-10.1	-68.2	126 ± 16	0.16
	310	76 ± 1	-29.3 ± 0.4	-9.7	-58.6	76 ± 12	0.28
	318	77 ± 2	-21.9 ± 0.5	-10.7	-32.6	76 ± 8	0.60
6.8	293	121 ± 1	-35.5 ± 0.3	-9.7	-81.2	nd	-
	298	128 ± 1	-27.3 ± 0.1	-10.7	-51.5	130 ± 15	0.68
	310	94 ± 3	-23.5 ± 0.5	-10.8	-38.1	71 ± 13	0.24
	318	94 ± 8	-15.9 ± 0.4	-11.7	-12.1	77 ± 7	0.3
7.4	293	127 ± 2	-38.3 ± 0.4	-9.6	-90.4	nd	-
	298	120 ± 1	-29.1 ± 0.2	-10.5	-57.7	111 ± 12	0.8
	310	107 ± 3	-23.3 ± 0.5	-11.2	-36.4	86 ± 17	0.2
	318	89 ± 2	-20.6 ± 0.4	-11.2	-27.6	75 ± 11	0.1
8.0	293	117 ± 1	-31.5 ± 0.2	-9.9	-67.8	nd	-
	298	111 ± 3	-33.4 ± 0.8	-9.8	-73.2	82 ± 7	0.06
	310	68 ± 2	-19.2 ± 0.4	-10.2	-26.8	69 ± 9	0.1
	318	81 ± 4	-19.2 ± 0.7	-11.0	-23.9	80 ± 8	0.6
10.0	293	76 ± 2	-12.8 ± 0.3	-10.4	-7.5	nd	-
	298	38 ± 1	-33.3 ± 1.0	-7.0	-81.2	25 ± 5	0.05
	310	26 ± 1	-28.6 ± 1.4	-6.7	-65.3	19 ± 2	0.20
	318	43 ± 7	-9.9 ± 1.4	-10.0	0.5	36 ± 5	0.20

**Table 2.** Chemical Shifts of  $^1\text{H}$  NMR of  $\beta$ -CD Protons in the Presence and Absence of Hydrochlorothiazide (HCT) at Different pH Values and at 298 K

pH	$\beta$ -CD	$H_1$	$H_2$	$H_3$	$H_4$	$H_5$	$H_6$
3.0	$\delta_{(\text{free})}$	5.058	3.642	3.956	3.570	3.840	3.869
	$\delta_{(\text{complex})}$	5.068	3.655	3.959	3.583	3.830	3.876
	$\Delta\delta^a$	0.010	0.013	0.003	0.013	-0.010	0.007
5.5	$\delta_{(\text{free})}$	5.078	3.658	3.974	3.592	3.859	3.887
	$\delta_{(\text{complex})}$	5.082	3.664	3.972	3.598	3.849	3.886
	$\Delta\delta^a$	0.004	0.007	-0.002	0.006	-0.010	-0.001
7.4	$\delta_{(\text{free})}$	5.064	3.648	3.962	3.577	3.846	3.875
	$\delta_{(\text{complex})}$	5.069	3.656	3.960	3.584	3.831	3.876
	$\Delta\delta^a$	0.005	0.008	-0.002	0.007	-0.016	0.001
8.0	$\delta_{(\text{free})}$	5.066	3.650	3.964	3.578	3.848	3.877
	$\delta_{(\text{complex})}$	5.069	3.656	3.960	3.584	3.831	3.876
	$\Delta\delta^a$	0.003	0.006	-0.003	0.006	-0.017	-0.001
8.7	$\delta_{(\text{free})}$	5.068	3.652	3.966	3.580	3.850	3.879
	$\delta_{(\text{complex})}$	5.072	3.658	3.964	3.586	3.834	3.879
	$\Delta\delta^a$	0.004	0.006	-0.002	0.006	-0.017	0.000
9.5	$\delta_{(\text{free})}$	5.070	3.653	3.969	3.582	3.853	3.881
	$\delta_{(\text{complex})}$	5.070	3.656	3.964	3.584	3.830	3.886
	$\Delta\delta^a$	-0.001	0.002	-0.005	0.002	-0.022	0.004
10.0	$\delta_{(\text{free})}$	5.064	3.648	3.964	3.577	3.848	3.876
	$\delta_{(\text{complex})}$	5.058	3.643	3.956	3.572	3.817	3.872
	$\Delta\delta^a$	-0.006	-0.004	-0.008	-0.005	-0.031	-0.003
12.0	$\delta_{(\text{free})}$	5.063	3.644	3.964	3.573	3.850	3.877
	$\delta_{(\text{complex})}$	5.065	3.651	3.963	3.579	3.824	3.879
	$\Delta\delta^a$	0.002	0.007	-0.001	0.006	-0.025	0.002

(Figure S1). It is a generally accepted fact that, when an aromatic guest is included in the CD cavity, the signals of the host inner protons ( $H_3$  and  $H_5$ ) suffer a significant upfield shift as a

consequence of the change in their chemical environment. Therefore, the shift deformation of the  $H_3$  and  $H_5$  proton peaks is highly sensitive to the formation of inclusion complexes.

**Table 3.** Chemical Shifts of  $^1\text{H}$  NMR of HCT Protons in the Presence and Absence of  $\beta$ -CD at Different pH Values and Temperatures (298 and 318 K)

pH	HCT	298 K			318 K		
		H <sub>1</sub>	H <sub>2</sub>	H <sub>3</sub>	H <sub>1</sub>	H <sub>2</sub>	H <sub>3</sub>
3.0	$\delta_{(\text{free})}$	8.259	7.094	—	8.478	7.329	5.091
	$\delta_{(\text{complex})}$	8.208	7.074	—	8.447	7.316	5.102
	$\Delta\delta^a$	<b>−0.051</b>	<b>−0.020</b>	—	<b>−0.031</b>	<b>−0.013</b>	<b>0.011</b>
5.5	$\delta_{(\text{free})}$	8.191	7.025	—	8.424	7.276	—
	$\delta_{(\text{complex})}$	8.220	7.086	—	8.468	7.336	—
	$\Delta\delta^a$	<b>0.029</b>	<b>0.060</b>	—	<b>0.045</b>	<b>0.060</b>	—
7.4	$\delta_{(\text{free})}$	8.188	7.029	4.798	8.415	7.274	5.036
	$\delta_{(\text{complex})}$	8.209	7.075	4.881	8.442	7.313	5.094
	$\Delta\delta^a$	<b>0.021</b>	<b>0.046</b>	<b>0.083</b>	<b>0.027</b>	<b>0.039</b>	<b>0.058</b>
8.0	$\delta_{(\text{free})}$	8.169	7.013	4.785	8.182	7.026	—
	$\delta_{(\text{complex})}$	8.199	7.067	4.875	8.423	7.296	—
	$\Delta\delta^a$	<b>0.030</b>	<b>0.054</b>	<b>0.090</b>	<b>0.244</b>	<b>0.270</b>	—
8.7	$\delta_{(\text{free})}$	8.194	7.041	—	8.396	7.253	5.034
	$\delta_{(\text{complex})}$	8.175	7.041	—	8.389	7.256	5.050
	$\Delta\delta^a$	<b>−0.020</b>	<b>0.000</b>	—	<b>−0.006</b>	<b>0.003</b>	<b>0.016</b>
9.5	$\delta_{(\text{free})}$	8.131	6.884	—	8.338	7.193	4.989
	$\delta_{(\text{complex})}$	8.138	6.945	—	8.345	7.202	5.006
	$\Delta\delta^a$	<b>0.007</b>	<b>0.061</b>	—	<b>0.007</b>	<b>0.010</b>	<b>0.017</b>
10.0	$\delta_{(\text{free})}$	8.033	6.884	—	8.259	7.112	4.914
	$\delta_{(\text{complex})}$	8.096	6.945	—	8.318	7.167	4.978
	$\Delta\delta^a$	<b>0.064</b>	<b>0.061</b>	—	<b>0.059</b>	<b>0.055</b>	<b>0.065</b>
12.0	$\delta_{(\text{free})}$	8.092	6.938	—	8.307	7.155	4.962
	$\delta_{(\text{complex})}$	8.104	6.953	—	8.325	7.174	4.985
	$\Delta\delta^a$	<b>0.012</b>	<b>0.015</b>	—	<b>0.017</b>	<b>0.019</b>	<b>0.023</b>

**Table 4.** Chemical Shifts of  $^1\text{H}$  NMR of  $\beta$ -CD Protons in the Presence and Absence of Hydrochlorothiazide at Different pH Values and at 318 K

pH	$\beta$ -CD	H <sub>1</sub>	H <sub>2</sub>	H <sub>3</sub>	H <sub>4</sub>	H <sub>5</sub>	H <sub>6</sub>
3.0	$\delta_{(\text{free})}$	5.2989	3.8810	4.1824	3.8014	4.0681	4.1065
	$\delta_{(\text{complex})}$	5.2897	3.8794	4.1524	3.7998	4.0751	4.1031
	$\Delta\delta^a$	<b>−0.008</b>	<b>−0.002</b>	<b>−0.030</b>	<b>−0.002</b>	<b>0.007</b>	<b>−0.003</b>
5.5	$\delta_{(\text{free})}$	5.3165	3.8986	4.2015	3.8242	4.0900	4.1248
	$\delta_{(\text{complex})}$	5.3139	3.8979	4.1965	3.8235	4.1009	4.1219
	$\Delta\delta^a$	<b>−0.003</b>	<b>−0.001</b>	<b>−0.005</b>	<b>−0.001</b>	<b>0.011</b>	<b>−0.003</b>
7.4	$\delta_{(\text{free})}$	5.2967	3.8839	4.1847	3.8038	4.0710	4.1091
	$\delta_{(\text{complex})}$	5.2910	3.8800	4.1762	3.8002	4.0760	4.1035
	$\Delta\delta^a$	<b>−0.006</b>	<b>−0.004</b>	<b>−0.008</b>	<b>−0.004</b>	<b>0.005</b>	<b>−0.006</b>
8.0	$\delta_{(\text{free})}$	5.2957	3.8824	4.1837	3.8026	4.0699	4.1080
	$\delta_{(\text{complex})}$	5.2907	3.8793	4.1761	3.7995	4.0759	4.1031
	$\Delta\delta^a$	<b>−0.005</b>	<b>−0.003</b>	<b>−0.008</b>	<b>−0.003</b>	<b>0.006</b>	<b>−0.005</b>
8.7	$\delta_{(\text{free})}$	5.2979	3.8840	4.1859	3.8045	4.0719	4.1100
	$\delta_{(\text{complex})}$	5.2911	3.8787	4.1774	3.7993	4.0772	4.1035
	$\Delta\delta^a$	<b>−0.007</b>	<b>−0.005</b>	<b>−0.008</b>	<b>−0.005</b>	<b>0.005</b>	<b>−0.007</b>
9.5	$\delta_{(\text{free})}$	5.2973	3.8824	4.1859	3.8037	4.0717	4.1093
	$\delta_{(\text{complex})}$	5.2911	3.8775	4.1792	3.7999	4.0776	4.1040
	$\Delta\delta^a$	<b>−0.006</b>	<b>−0.005</b>	<b>−0.007</b>	<b>−0.005</b>	<b>0.006</b>	<b>−0.005</b>
10.0	$\delta_{(\text{free})}$	5.2780	3.8629	4.1699	3.7849	4.0534	4.0900
	$\delta_{(\text{complex})}$	5.2897	3.8759	4.1807	3.7969	4.0759	4.1039
	$\Delta\delta^a$	<b>0.012</b>	<b>0.013</b>	<b>0.013</b>	<b>0.012</b>	<b>0.023</b>	<b>0.014</b>
12.0	$\delta_{(\text{free})}$	5.2972	3.8805	4.1884	3.8023	4.0754	4.1126
	$\delta_{(\text{complex})}$	5.2958	3.8822	4.1867	3.8033	4.0820	4.1101
	$\Delta\delta^a$	<b>−0.001</b>	<b>0.002</b>	<b>−0.002</b>	<b>0.001</b>	<b>0.007</b>	<b>−0.003</b>

The  $^1\text{H}$  shifts of the guest may be different, either positive or negative, depending on the position of the protons within the cavity.

From Table 2, it can be seen that at 298 K the H<sub>3</sub> and H<sub>5</sub> protons exhibited displacements in their  $\delta$  in the presence of

the drug, thus confirming the formation of an inclusion complex. The upfield shift of H<sub>5</sub>, located on the inner surface at the primary hydroxyl group side, was the most prominent at all pH values assayed. Because of the higher shielding effect on the H<sub>5</sub> proton with respect to H<sub>3</sub>, it can be hypothesized that there was

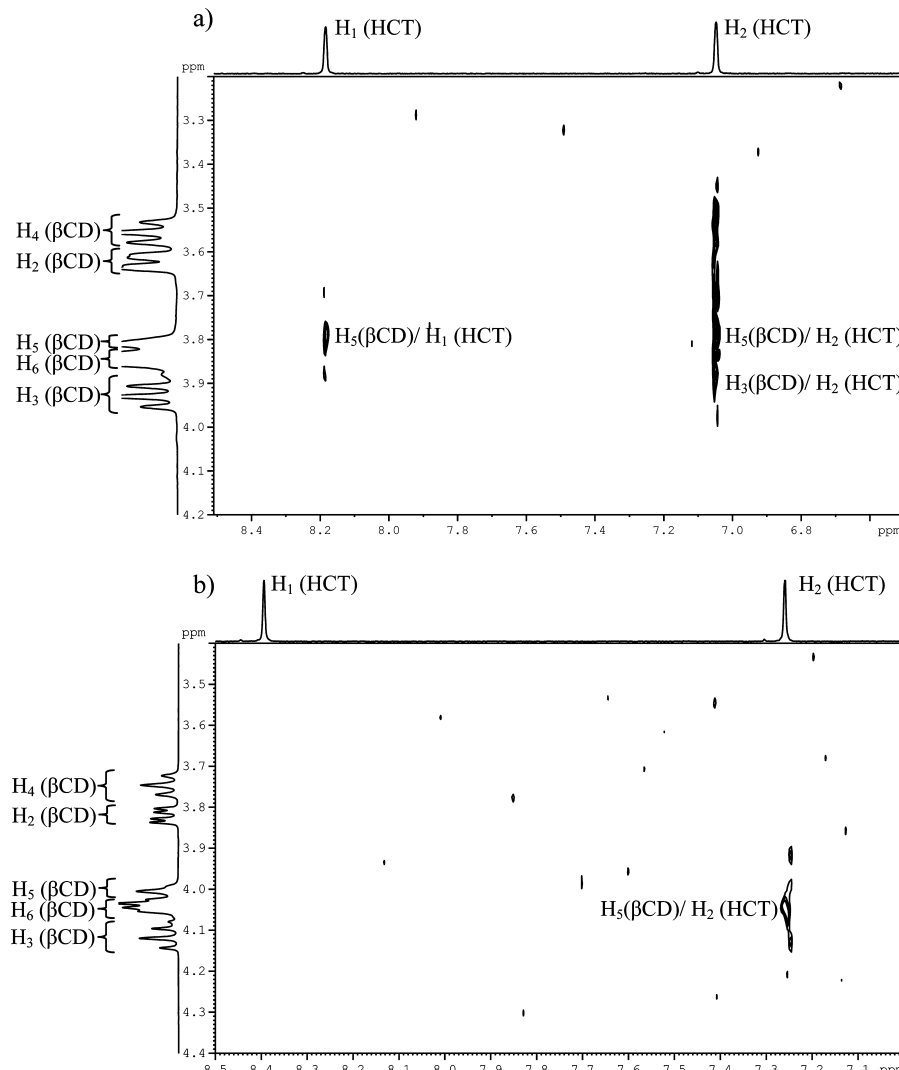


**Figure 3.** Expanded region of the 2D-ROESY spectrum of (a) HCT:β-CD in D<sub>2</sub>O at 298 K and (b) HCT:β-CD in D<sub>2</sub>O at 318 K.

a very deep penetration of the drug into the CD cavity. In addition, the chemical shifts corresponding to the protons located at the outer surface of β-CD (H<sub>1</sub>, H<sub>2</sub>, H<sub>6</sub>, and H<sub>4</sub>) were also modified, which could have been due to a conformational rearrangement in the host molecule.

All spins of HCT experienced chemical shift changes upon complexation, suggesting a total inclusion of HCT into the β-CD cavity (Table 3). However, the H<sub>3</sub> proton signal of HCT could not be determined at all pH values due to overlap with the remaining peak of the saturated water. At 318 K (Tables 3 and 4), it could be observed that lower  $\Delta\delta$  occurred, which suggests a lower stability of the inclusion complex.

In order to study the complex dynamics, the average intermolecular distances and the cross-peak intensities between the host and guest molecules, two-dimensional ROESY or NOESY experiments were performed. Figure 3 shows the ROESY expansion contour map for the HCT:β-CD system in D<sub>2</sub>O (~pH 5) at 298 and 318 K, with results at 298 K (Figure 3a) showing that H<sub>5</sub> of β-CD shared ROE's with protons H<sub>1</sub> (weak) and H<sub>2</sub> (strong) of HCT, while H<sub>3</sub> of the β-CD shared ROE's with H<sub>2</sub> (strong) of HCT. This evidence suggests that the HCT positioning was not perpendicular to the axis of the β-CD hydrophobic cavity, with H<sub>2</sub> facing the inner surface of β-CD while H<sub>1</sub> faced the exterior of the cavity. In order to test

the complex stability, the ROESY spectrum at 318 K was recorded and it was demonstrated that the correlation spots disappeared at this temperature (Figure 3b), which was consistent with the lower affinity of the complex determined by ITC (Table 1).

**Phase Solubility Studies.** Phase solubility diagrams are useful tools to study inclusion complexes between poorly soluble compounds and cyclodextrins, since they not only provide a quantitative measure of the solubilizing ability of the host but also allow the corresponding stability constant to be calculated by analyzing the solubility curves.<sup>38</sup> Figure 4 shows the phase solubility diagrams of HCT with β-CD in aqueous solutions determined at various pH values and at different temperatures. In all cases, the solubility of HCT increased linearly as the molar concentration of β-CD was raised, supporting the formation of soluble 1:1 HCT:β-CD complexes over the concentration range studied, which in turn defined the A<sub>L</sub> type solubility diagrams. The apparent stability constants ( $K_{1:1}$ ) of the inclusion complexes were calculated from the linear fit of the curve and using eq 2 at different pH values and temperatures and are presented in Table 1. As can be seen, the observed affinity was highly dependent on the ionization state of HCT, with lower  $K_{1:1}$  values occurring at higher pH values. The molecular basis of this may be related to the decrease in HCT hydrophobicity, which in turn may affect the establishment of

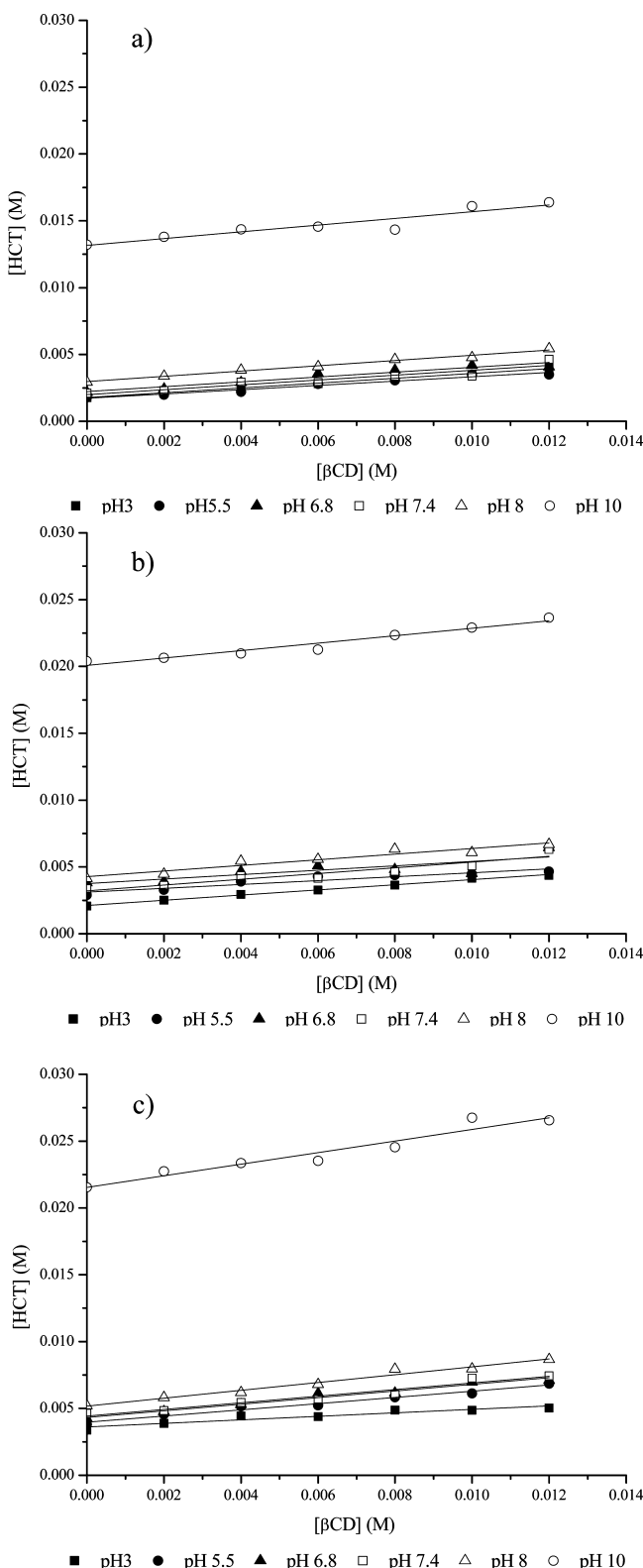


**Figure 4.** Phase solubility diagrams of HCT with  $\beta$ -CD in different buffer solutions at (a) 298 K, (b) 310 K, and (c) 318 K.

intermolecular van der Waals contacts and raise the ligand desolvation energy required for complexation to occur.

The temperature dependence of affinity was also studied from these phase solubility diagrams, with Figure S2 in the Supporting Information showing the corresponding van't Hoff plots for the association processes between HCT and  $\beta$ -CD.

The linear relationship of the  $R \ln K$  vs  $1/T$  data indicates the independence of  $\Delta H^\circ$  and  $\Delta S^\circ$  with respect to  $T$  ( $\Delta C_p^\circ \sim 0$ ), while the absence of a behavior reveal that  $\Delta H^\circ$  and  $\Delta S^\circ$  are temperature dependent and related to an association process with  $\Delta C_p^\circ \neq 0$ . From Figure S2, it is clear that the van't Hoff plots are not linear, and thus the use of the nonlinear form of the van't Hoff equation to estimate  $\Delta H^\circ$ ,  $\Delta S^\circ$ , and  $\Delta C_p^\circ$  may be risky, given the uncertainty of the  $K$  values. Consequently, direct calorimetric studies are necessary to provide a complete thermodynamic description of the system.

**Molecular Modeling Studies. Docking Assays.** The docking of the ligand (HCT) to  $\beta$ -CD was performed by considering its three possible ionization states, obtaining in all cases two alternate binding poses in which ring A or ring B was deeply buried into the  $\beta$ -CD hydrophobic cavity.

Figure 5 shows the two alternate poses obtained for the neutral species of HCT. In binding pose-1 (Figure 5a), the

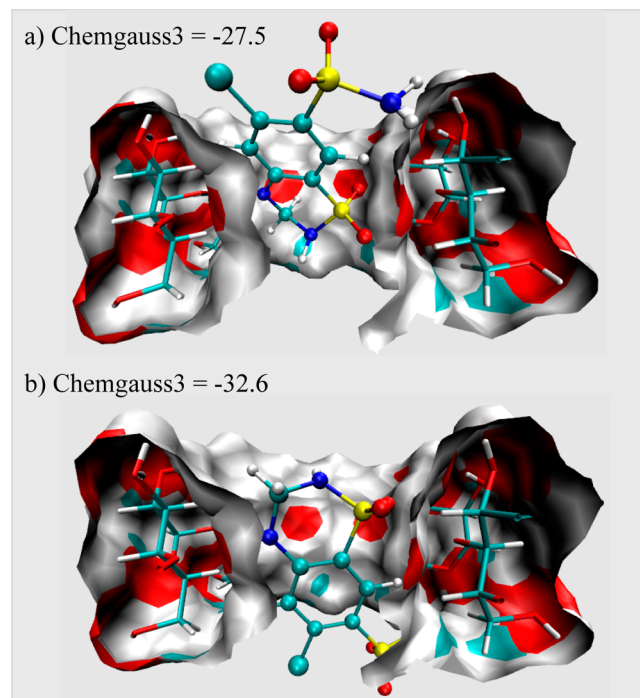


**Figure 5.** Three-dimensional representations of the binding modes between neutral HCT and  $\beta$ -CD as predicted by molecular docking: (a) pose-1; (b) pose-2. The values shown correspond to the scoring value (dimensionless) determined by the Chemgauss3 scoring function.

benzothiadiazine ring (ring B) of HCT was deeply inserted into the  $\beta$ -CD cavity, while in the binding pose-2 (Figure 5b) the chlorobenzyl moiety (ring A) was inserted into the hydrophobic cavity and oriented toward the narrower rim of  $\beta$ -CD. There were no significant differences between the scoring values assigned by ChemGauss3 for both poses (-27.5 and -32.6, for pose-1 and pose-2, respectively), and thus it was not possible by means of this rigid docking approach to definitively discriminate which of these two inclusion modes was the more stable. The chemical shifts displacements quantified by NMR in the protons located in the outer surface of  $\beta$ -CD ( $H_2$  and  $H_4$ ) evidenced that after complexation a conformational change in the guest molecule occurred (Table 2). This observation strongly suggests that marked induced fit phenomena took

place when HCT was included into the  $\beta$ -CD structure. Considering that the molecular docking procedure was performed over the native structure of  $\beta$ -CD (BCDEXD10, i.e., unliganded), it was not expected that by applying a rigid docking approach over the native  $\beta$ -CD to predict the initial conformation of the complex, it will be possible to propose a refined intermolecular interaction pattern that is consistent with the observed experimental affinity. In this way, further refinements by molecular dynamics methods are needed.

Regarding the mono- and di-ionized form of HCT (Figures 6 and 7, respectively), a similar behavior to that described for

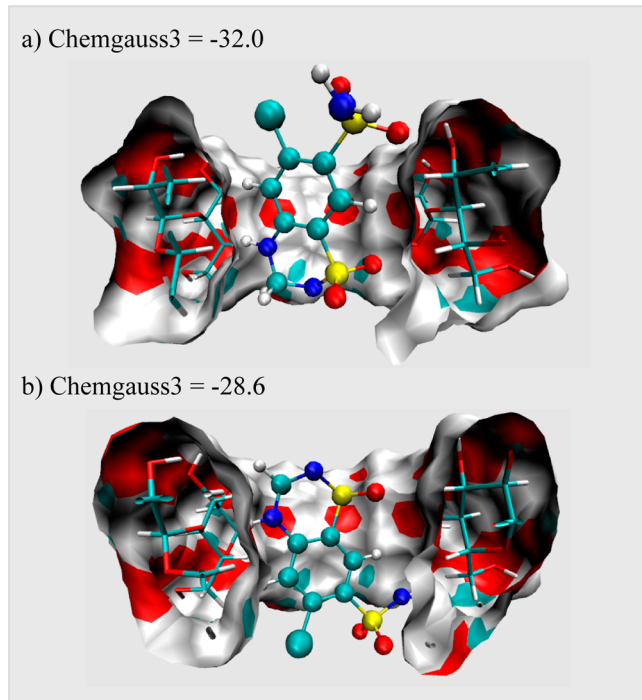


**Figure 6.** Three-dimensional representations of the binding modes between monoionized HCT and  $\beta$ -CD as predicted by molecular docking: (a) pose-1; (b) pose-2. The values shown correspond to the scoring value (dimensionless) determined by the Chemgauss3 scoring function.

neutral HCT was observed, with two alternate binding poses being found and similar scoring values determined by ChemGauss3.

Although the molecular docking studies confirmed that HCT fitted into the  $\beta$ -CD cavity, it has been previously reported that this technique is not precise enough to definitively assess the conformation of the inclusion complex,<sup>31,32</sup> and consequently it would not be safe to correlate the binding poses observed with the experimental results. However, docking methods are useful to predict the initial pose of the complex, which may then be subjected to further refinement by molecular dynamics methods, in which the flexibility of the receptor ( $\beta$ -CD) is taken into account and the effect of temperature and solvent is also modeled.

**Molecular Dynamics Assays.** The complexes shown in Figures 5–7 were subjected to molecular dynamics simulations under the conditions described in the material and methods section. After the production phase was completed, structural alignment throughout the simulated trajectory was performed, and the rmsd vs time profiles were constructed using as a reference the initial complex obtained by molecular docking

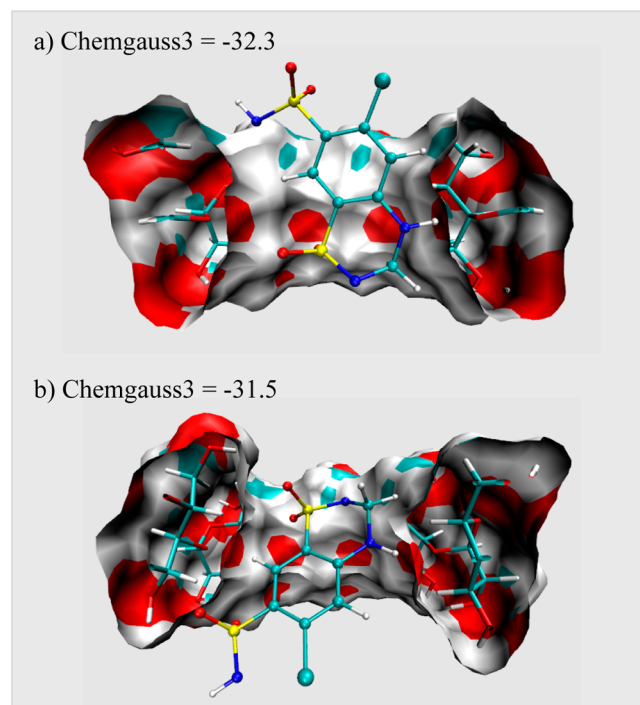


**Figure 7.** Three-dimensional representations of the binding modes between di-ionized HCT and  $\beta$ -CD as predicted by molecular docking: (a) pose-1; (b) pose-2. The values shown correspond to the scoring value (dimensionless) determined by the Chemgauss3 scoring function.

(Figures S3, S4, and S5 in the Supporting Information). In all cases, when molecular dynamics conditions were applied to the complexes obtained by molecular docking, a significant conformational rearrangement was observed in the host molecule (rmsd between 2 and 4 Å), which was consistent with the  $\Delta\delta$  calculated for  $H_1$ ,  $H_2$ ,  $H_6$ , and  $H_4$  from the NMR experiments (Table 2).

Figure S3 shows the rmsd vs time profiles for both docking poses corresponding to neutral HCT, in which it can be seen that the structural rearrangement took place during the heating and equilibration phase (0–5000 steps), with an equilibrium in the structure reached between 6 and 10 ns of simulation (35 000–55 000 steps). In order to discriminate the most stable binding pose among the two docking poses analyzed, energetic decomposition analyses were performed in this time frame (6–10 ns), with the corresponding results presented in Table 5. It can be observed for the neutral HCT that the most stable inclusion mode was pose-1, which exhibited a higher electrostatic interaction component than pose-2 (-18.1 and -12.0 kcal/mol, respectively). The representative conformation for this binding mode is presented in Figure 8a, which shows that the main driving force for the complex formation constituted a hydrogen bond interaction between the oxygen of the sulfonamide moiety and the C-3 hydroxyl group from  $\beta$ -CD. This intermolecular interaction was formed at around 6 ns and persisted throughout the simulation (Figure S6 in the Supporting Information). This predicted binding pose was consistent with  $\Delta\delta$  as determined by NMR studies (Table 2), in which a deshielding effect (positive  $\Delta\delta$ ) was produced on  $H_3$  by the electronegativity of the sulfonamide moiety, while a shielding effect on  $H_5$  (negative  $\Delta\delta$ ) was produced by the electron-rich system of ring B that was deeply buried into the  $\beta$ -CD cavity.

**Table 5. Results Obtained for the Energetic Decomposition Analyses from the Molecular Dynamics Trajectories**

HCT species	T (K)	elect <sup>a</sup>	vdW <sup>b</sup>	gas <sup>c</sup>	solv <sup>d</sup>	ΔG <sup>e</sup>
HCT-neutral pose-1	298	-18.1	-24.5	-42.7	23.5	-19.1
	310	-14.0	-27.9	-42.0	23.8	-18.2
	318	-10.9	-26.3	-37.2	21.2	-16.0
HCT-neutral pose-2	298	-12.0	-25.9	-37.9	21.9	-16.0
HCT-monoionized pose-1	298	-25.8	-25.4	-50.5	38.7	-11.8
HCT-monoionized pose-2	298	-26.8	-24.4	-51.2	36.0	-15.2
	310					
	318					
HCT-di-ionized pose-1	298	-77.1	-24.4	-101.4	88.6	-12.8
	310					
	318					
HCT-di-ionized pose-2	298	-66.2	-16.3	-82.5	73.4	-9.2

<sup>a</sup>Electrostatic interaction component (kcal/mol). <sup>b</sup>van der Waals interaction component (kcal/mol). <sup>c</sup>Interaction energy in the gas phase (kcal/mol). <sup>d</sup>Solvation energy (kcal/mol). <sup>e</sup>Estimated binding energy (kcal/mol).

When the binding mode of the monoionized form of HCT was analyzed (Figure 8b), the rmsd vs time plots showed that the complex corresponding to pose-1 remained relatively stabilized after the heating and equilibration phase, while pose-2 exhibited a higher structural variability than pose-1 (Figure S4 in the Supporting Information). After energetic decomposition analyses were performed (5000–55 000 steps), it was found that pose-2 exhibited a higher affinity than pose-1 (-15.2 and -11.8 kcal/mol, respectively), with both monoionized docking poses exhibiting lower affinities than the neutral species. From the corresponding cluster analysis of the pose-2 MD trajectory, the most populated conformation was obtained (Figure 8b), which was significantly different from that obtained for neutral HCT (Figure 8a) since the sulfonamide moiety was now oriented toward the narrower rim of  $\beta$ -CD, with the amino group establishing stable hydrogen bond interactions with the oxygen of the 1,4 glycosidic bridge (Figure S7 in the Supporting Information). The proximity of the amino group to  $H_3$  and  $H_5$ , along with the insertion of the aromatic ring into the hydrophobic cavity, is consistent with the shielding effect observed by NMR for both atoms (Table 2).

Regarding the di-ionized species of HCT, the rmsd vs time plot (Figure S5 in the Supporting Information) again showed a significant rearrangement of the initial complex, with equilibrium

reached after 6 ns (30 000 steps) of simulation. An energetic decomposition analysis was performed between 3 and 6 ns of simulation (Table 5), which revealed that pose-1 exhibited a higher affinity than pose-2 (-12.8 and -9.2 kcal/mol, respectively), with this species exhibiting a lower affinity than either the monoionized or neutral species of HCT. The clustered structure of pose-1 (Figure 8c) showed that HCT was deeply buried into the  $\beta$ -CD cavity and established hydrogen bond interactions in both the wide and narrow rims of the host molecule (Figure S8 in the Supporting Information). The high shielding effect on  $H_3$  and  $H_5$  observed in the NMR spectra was attributed to the perpendicular disposition of the electron-rich aromatic ring with respect to the inner  $\beta$ -CD protons.

From the results above, it can be seen that the predicted affinities for the three HCT ionization states analyzed are in agreement with the experimental observations obtained by ITC and DSP (Table 1). Therefore, we can hypothesize that the affinity of HCT diminished as the degree of ionization of the ligand increased as a consequence of the higher energy required to desolvate the ionized HCT (Table 5). It is noteworthy that the energetic stabilization derived from the van der Waals interactions remained essentially unchanged. In line with these observations, the idea that the solvation energies may limit the overall observed affinities in the  $\beta$ -CD inclusion complexes has already been reported by our research group.<sup>31,32</sup>

**Affinity versus Temperature.** The effect of temperature on HCT affinity was studied by both experimental and theoretical methods. As a general overview, the observed affinity was highly dependent on the HCT ionization state, with a marked decrease occurring for neutral HCT at higher temperatures (Table 1), while the changes in affinity were not significant for either mono- or di-ionized HCT. These results suggest that the dependence of affinity on temperature originates from differences in the inclusion mode of HCT within the  $\beta$ -CD cavity. Table 1 presents the affinity constants obtained by phase solubility and ITC analyses, while Table 5 presents the corresponding energetic components as determined from the molecular dynamics trajectories using different temperatures for the most stable HCT inclusion mode. It can be observed that, for neutral HCT, the electrostatic component was highly dependent on temperature, with a marked decrease as the temperature rose (-18.1, -14.0, and -10.9 kcal/mol at 298, 310, and 318 K, respectively), which was consistent with the decrease in  $\Delta H$  values determined by ITC (Table 1). This finding also suggests that, as the temperature is raised, HCT was not excluded from the  $\beta$ -CD, as shown by the fact that the

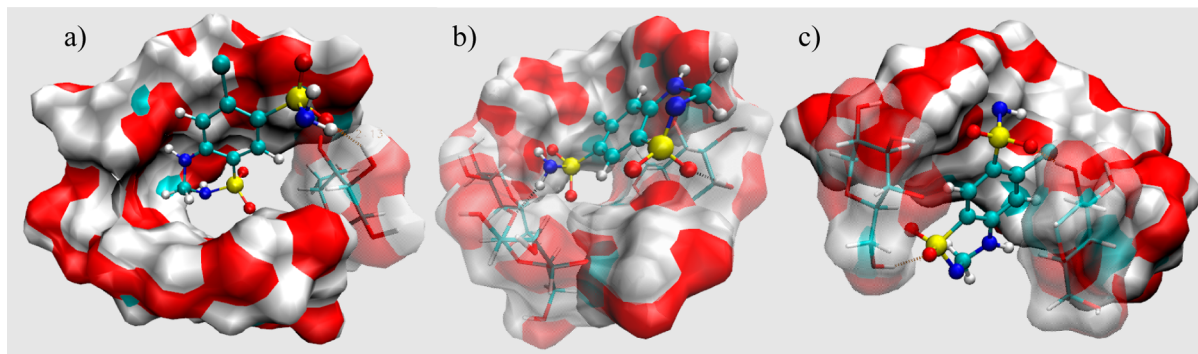


**Figure 8.** Three-dimensional array of the binding mode between  $\beta$ -CD and (a) neutral HCT, (b) monoionized HCT, and (c) di-ionized HCT. The structures represent the most frequent conformation as determined by a clustering algorithm based on the rmsd of the corresponding molecular dynamics trajectories.

van der Waals component remained unchanged ( $-24.5$ ,  $-27.9$ , and  $-26.3$  kcal/mol at 298, 310, and 318 K, respectively). The hydrogen-bonding analyses demonstrated a significant change in the pattern of hydrogen bonds formed at different temperatures for this complex, with the main hydrogen bond interaction being established between the oxygen ( $O_2$ ) of the sulfonamide group and the  $C_3OH$  from the wider rim of  $\beta$ -CD at 298 K (occupancy 27.7%) (Figure S9a in the Supporting Information). At 310 K, neutral HCT was deeply buried into the  $\beta$ -CD cavity, and in this case the main hydrogen bond contact was established between the NH group of the benzothiadiazine ring and O6 of  $\beta$ -CD (Figure S9b). A significantly lower occupancy was calculated (16.7%), which in turn led to a decrease in the electrostatic component compared to that at 298 K ( $-14.0$  and  $-18.1$  kcal/mol, respectively). At the higher assayed temperature (318 K), the hydrogen bond interaction between the sulfonamide moiety of HCT and the OH from the wider rim of  $\beta$ -CD was again identified as the main stabilizing contact (Figure S9c). This interaction exhibited the lowest occupancy of the three studied temperatures (8.2%), which was consistent with the significant drop in affinity.

When HCT in its monoionized form was analyzed (Figure S10 in the Supporting Information), no significant changes in the three-dimensional array of the complex were observed as a consequence of raising the temperature. The hydrogen bond analyses showed that in all cases stable hydrogen bond interactions were established between the oxygen of the sulfonamide group and the C-3 OH from the wider rim of  $\beta$ -CD, whose occupancy did not exhibit temperature dependence (70.9, 76.5, and 68.1% at 298, 310, and 318 K, respectively). This observation was consistent with the stability of the electrostatic component calculated at the three assayed temperatures (Table 5). Based on the HCT  $pK_a$  values, it can be considered that this monoionized species was mostly present between pH 8 and 9, which was consistent with the relatively constant affinity values reported in Table 1 for this pH range. Finally, the di-ionized species of HCT (Figure S11 in the Supporting Information) exhibited a similar trend to that observed for the monoionized species, with stable hydrogen bonds being formed at both the wide and narrow rims of the  $\beta$ -CD molecule, which was again in agreement with the experimental affinity values determined at pH 10.

## CONCLUSIONS

Supramolecular complexes of HCT and  $\beta$ -CD were prepared and fully characterized using isothermal titration calorimetry (ITC),  $^1H$  NMR spectroscopy, phase solubility diagrams, and molecular modeling methods. A “one-binding site” model was used to evaluate the ITC results, which demonstrated the formation of a 1:1 HCT: $\beta$ -CD inclusion complex, with an enthalpy-driven exothermic behavior. The influence of pH and temperature on HCT affinity was carefully analyzed and discussed at a molecular level, with a good agreement being found between the experimental and theoretical methods. In this way, the increase in the ionization state of HCT caused its affinity for  $\beta$ -CD to be lowered, which was consistent with the raised energetic cost of desolvating hydrated HCT ionic species. Regarding the temperature effect, lower affinity constants were quantified as the temperature increased in the 298–318K range, a phenomenon that was attributed to modifications in the hydrogen-bonding network between the ligand and the  $\beta$ -CD molecule. This effect was highly dependent on the HCT ionization state, with a marked decrease in affinity occurring for neutral HCT. In summary, from

the presented studies we can conclude that the analysis of the ionization state and temperature dependence of the affinity of a guest molecule to  $\beta$ -CD is crucial for the rational design of new materials based on self-assembly chemistry. The understanding and accurate characterization of these aspects in the design of CD complexes with pharmaceutical applications is of particular interest.

## ASSOCIATED CONTENT

### S Supporting Information

Depiction of the three-dimensional structure of  $\beta$ -CD, showing the hydrophobic cavity and proton numbering, van't Hoff plots for the association of HCT with  $\beta$ -CD, rmsd vs time plot, hydrogen bond distances, and hydrogen bond analysis. This material is available free of charge via the Internet at <http://pubs.acs.org>.

## AUTHOR INFORMATION

### Corresponding Author

\*E-mail: glagra@fcq.un.edu.ar. Tel./Fax: 54-351-4334163; 54-351-4334127.

### Notes

The authors declare no competing financial interest.

## ACKNOWLEDGMENTS

The authors thank FONCyT (Préstamo BID 1728/OC-AR, PICT 1376), the Secretaría de Ciencia y Técnica de la Universidad Nacional de Córdoba (SECyT), and the Consejo Nacional de Investigaciones Científicas y Tecnológicas de la Nación (CONICET) for their financial support. We also thank Ferromet S.A. (agent of Roquette in Argentina) for their donation of  $\beta$ -cyclodextrin. We are grateful to Dr. Gloria M. Bonetto for NMR measurements and for her helpful discussion of the  $^1H$  NMR spectra. M.A.Q. acknowledges the GPGPU Computing Group and Dr. Nicolás Wolovick from the Facultad de Matemática, Astronomía y Física (FAMAF), Universidad Nacional de Córdoba, Argentina, for providing access to computing resources.

## REFERENCES

- (1) Loftsson, T.; Brewster, M. E. *J. Pharm. Sci.* **2012**, *101* (9), 3019–3032.
- (2) Serno, T.; Geidobler, R.; Winter, G. *Adv. Drug Delivery Rev.* **2011**, *63* (13), 1086–1106.
- (3) Laza-Knoerr, A. L.; Gref, R.; Couvreur, P. *J. Drug Target.* **2010**, *18* (9), 645–656.
- (4) Carrier, R. L.; Miller, L. A.; Ahmed, I. *J. Controlled Release* **2007**, *123* (2), 78–99.
- (5) Loftsson, T.; Duchêne, D. *Int. J. Pharm.* **2007**, *329* (1–2), 1–11.
- (6) Villalonga, R.; Cao, R.; Fragoso, A. *Chem. Rev.* **2007**, *107*, 3088–3116.
- (7) Astray, G.; Gonzalez-Barreiro, C.; Mejuto, J. C.; Rial-Otero, R.; Simal-Gándara, J. *Food Hydrocolloids* **2009**, *23* (7), 1631–1640.
- (8) Cravotto, G.; Binello, A.; Baranelli, E.; Carraro, P.; Trotta, F. *Curr. Nutr. Food Sci.* **2006**, *2* (4), 343–350.
- (9) Maeztu, R.; Tardajos, G.; Gonzalez-Gaitano, G. *J. Phys. Chem. B* **2010**, *114*, 2798–2806.
- (10) Centini, M.; Maggiore, M.; Casolari, M.; Andreassi, M.; Maffei Facino, R.; Anselmi, C. *J. Inclusion Phenom. Macrocyclic Chem.* **2007**, *57* (1–4), 109–112.
- (11) Fakayode, S. O.; Lowry, M.; Fletcher, K. A.; Huang, X.; Powe, A. M.; Warner, I. M. *Curr. Anal. Chem.* **2007**, *3* (3), 171–181.
- (12) Liu, L.; Guo, Q. X. *J. Inclusion Phenom.* **2002**, *42* (1–2), 1–14.
- (13) Zhang, H.; Tan, T.; Feng, W.; Van Der Spoel, D. *J. Phys. Chem. B* **2012**, *116*, 12684–12693.

- (14) Chen, Y.; Li, F.; Liu, B. W.; Jiang, B. P.; Zhang, H. Y.; Wang, L. H.; Liu, Y. *J. Phys. Chem. B* **2010**, *114*, 16147–16155.
- (15) Jana, M.; Bandyopadhyay, S. *J. Phys. Chem. B* **2011**, *115*, 6347–6357.
- (16) Harries, D.; Rau, D. C.; Parsegian, V. A. *J. Am. Chem. Soc.* **2005**, *127*, 2184–2190.
- (17) Asandei, A.; Mereuta, L.; Luchian, T. *J. Phys. Chem. B* **2011**, *115*, 10173–10181.
- (18) Challa, R.; Ahuja, A.; Ali, J.; Khar, R. K. *AAPS PharmSciTech [electronic resource]* **2005**, *6* (2), E329–357.
- (19) Khalil, S. K. H.; El-Feky, G. S.; El-Banna, S. T.; Khalil, W. A. *Carbohydr. Polym.* **2012**, *90* (3), 1244–1253.
- (20) Jug, M.; Kosalec, I.; Maestrelli, F.; Mura, P. *Carbohydr. Polym.* **2012**, *90* (4), 1794–1803.
- (21) Finger, S.; Wiegand, C.; Buschmann, H. J.; Hippler, U. C. *Int. J. Pharm.* **2012**, *436* (1–2), 851–856.
- (22) Nguyen, T. A.; Liu, B.; Zhao, J.; Thomas, D. S.; Hook, J. M. *Food Chem.* **2013**, *136* (1), 186–192.
- (23) Martins, M. H.; Calderini, A.; Pessine, F. B. T. *J. Inclusion Phenom. Macrocyclic Chem.* **2012**, *74* (1–4), 109–116.
- (24) Jug, M.; Maestrelli, F.; Mura, P. *J. Inclusion Phenom. Macrocyclic Chem.* **2012**, *74* (1–4), 87–97.
- (25) Messerli, F. H.; Bangalore, S. *Am. J. Med.* **2011**, *124* (10), 896–899.
- (26) Chen, M. L.; Amidon, G. L.; Benet, L. Z.; Lennernas, H.; Yu, L. X. *Pharm. Res.* **2011**, *28* (7), 1774–1778.
- (27) Trivedi, R. V.; Admane, P. S.; Taksande, J. B.; Mahore, J. G.; Umekar, M. *J. Pharm. Lett.* **2011**, *3* (6), 8–17.
- (28) Veena, G.; Saritha, M. *J. Chem. Pharm. Res.* **2011**, *3* (4), 150–158.
- (29) Denadai, A. M. L.; Santoro, M. M.; Silva, L. H. D.; Viana, A. T.; Santos, R. A. S.; Sinisterra, R. D. *J. Inclusion Phenom. Macrocyclic Chem.* **2006**, *55* (1–2), 41–49.
- (30) Hansen, L. D.; Fellingham, G. W.; Russell, D. *J. Anal. Biochem.* **2011**, *409* (2), 220–229.
- (31) Zoppi, A.; Quevedo, M. A.; Delrivo, A.; Longhi, M. R. *J. Pharm. Sci.* **2010**, *99* (7), 3166–3176.
- (32) Zoppi, A.; Quevedo, M. A.; Longhi, M. R. *Bioorg. Med. Chem.* **2008**, *16* (18), 8403–8412.
- (33) Boonyaratpanakalin, K.; Wolschann, P.; Toochinda, P.; Lawtrakul, L. *Eur. J. Pharm. Sci.* **2012**, *47* (4), 752–758.
- (34) Sivasankar, T.; Antony Muthu Prabhu, A.; Karthick, M.; Rajendiran, N. *J. Mol. Struct.* **2012**, *1028*, 57–67.
- (35) Tallury, S. S.; Smyth, M. B.; Cakmak, E.; Pasquinelli, M. A. *J. Phys. Chem. B* **2012**, *116*, 2023–2030.
- (36) Raffaini, G.; Ganazzoli, F. *J. Phys. Chem. B* **2010**, *114*, 7133–7139.
- (37) Raffaini, G.; Ganazzoli, F.; Malpezzi, L.; Fuganti, C.; Fronza, G.; Panzeri, W.; Mele, A. *J. Phys. Chem. B* **2009**, *113*, 9110–9122.
- (38) Hemmateenejad, B.; Emami, L.; Sharghi, H. *Spectrochim. Acta A: Mol. Biomol. Spectrosc.* **2010**, *75* (1), 340–346.
- (39) Allouche, A. R. *J. Comput. Chem.* **2011**, *32* (1), 174–182.
- (40) Gaussian 03, Revision C.02: Frisch, M. J.; Trucks, G. W.; Schlegel, H. B.; Scuseria, G. E.; Robb, M. A.; Cheeseman, J. R.; Montgomery, J. A.; Vreven, Jr., T.; Kudin, K. N.; Burant, J. C., et al., Gaussian, Inc., Wallingford CT, 2004.
- (41) OpenEye Scientific Software, [www.eyesopen.com](http://www.eyesopen.com).
- (42) Hawkins, P. C. D.; Skillman, A. G.; Warren, G. L.; Ellingson, B. A.; Stahl, M. T. *J. Chem. Inf. Model.* **2010**, *50* (4), 572–584.
- (43) Omega, 2.4.3. OpenEye Scientific Software, Santa Fe, NM; <http://www.eyesopen.com>.
- (44) McGann, M. *J. Comput. Aided Mol. Des.* **2012**, *8* (26), 1–10.
- (45) McGann, M. *J. Chem. Inf. Model.* **2011**, *51* (3), 578–596.
- (46) Fred, 2.2.5. OpenEye Scientific Software, Santa Fe, NM; <http://www.eyesopen.com>.
- (47) VIDA, 4.1.2. OpenEye Scientific Software, Santa Fe, NM; <http://www.eyesopen.com>.
- (48) Case, D. A.; Cheatham, T. E., III; Darden, T.; Gohlke, H.; Luo, R.; Merz, K. M., Jr.; Onufriev, A.; Simmerling, C.; Wang, B.; Woods, R. *J. Comput. Chem.* **2005**, *26* (16), 1668–1688.
- (49) Wang, J.; Wolf, R. M.; Caldwell, J. W.; Kollman, P. A.; Case, D. A. *J. Comput. Chem.* **2004**, *25* (9), 1157–1174.
- (50) Kirschner, K. N.; Yongye, A. B.; Tschaepel, S. M.; González-Outeiriño, J.; Daniels, C. R.; Foley, B. L.; Woods, R. *J. Comput. Chem.* **2008**, *29* (4), 622–655.
- (51) Kuhn, B.; Gerber, P.; Schulz-Gasch, T.; Stahl, M. *J. Med. Chem.* **2005**, *48*, 4040–4048.
- (52) Humphrey, W.; Dalke, A.; Schulten, K. *J. Mol. Graph.* **1996**, *14* (1), 33–38.
- (53) Turnbull, W. B.; Daranas, A. H. *J. Am. Chem. Soc.* **2003**, *125* (48), 14859–14866.
- (54) Indyk, L.; Fisher, H. F. Theoretical aspects of isothermal titration calorimetry. In *Methods in Enzymology*; Gary, K., Ackers, M. L. J., Eds.; Academic Press: New York, 1998; Vol. 295, Chapter 17, pp 350–364.
- (55) Crupi, V.; Majolino, D.; Venuti, V.; Guella, G.; Mancini, I.; Rossi, B.; Verrocchio, P.; Viliani, G.; Stanganelli, R. *J. Phys. Chem. A* **2010**, *114*, 6811–6817.